Ultrasonic investigation of granular superconducting films

J. Schmidt* and M. Levy
Department of Physics, University of Wisconsin–Milwaukee, Milwaukee, Wisconsin 53201

A. F. Hebard
AT&T Bell Laboratories, Murray Hill, New Jersey 07974
(Received 24 May 1990)

The dc resistance and surface-acoustic-wave (SAW) attenuation has been measured in granular Pb/PbO_x and In/InO_x films as a function of temperature. The behavior of resistance and attenuation data has been found to be in agreement with the predictions of a recently developed model that is based on a percolation description of granular superconducting films. In this paper we will present the resistance and SAW attenuation data and compare them to the predictions of the percolation model.

I. INTRODUCTION

Previously, a model has been developed[1] to account for the excess surface-acoustic-wave (SAW) attenuation that was observed in a granular superconducting Pb/PbO_x film as the film entered the superconducting state. This model, based on a percolation description of granular superconductors,[2,3] was found to give qualitative agreement with the observed SAW attenuation for the granular Pb/PbO_x film. The model could also be used to describe the dc resistance of the film; however, it was found that the agreement between the predicted dc resistance and the observed resistance for the Pb/PbO_x film was not very good.

We have recently obtained additional data on the dc resistance and SAW attenuation for the granular Pb/PbO_x film as well as for some granular In/InO_x films. The SAW attenuation data appear to give further support for the percolation model of Ref. 1. In addition, calculations using a detailed model for the resistance distribution function in the superconducting state have been done for the dc resistance that is predicted by the percolation model. These calculations appear to provide better agreement between the model and the resistance data. In this paper we shall present the experimental data that were obtained on the Pb/PbO_x and InO_x films and discuss the data in terms of the percolation model. The remainder of this paper is organized as follows. In Sec. II we present the SAW attenuation data and dc resistance data that were obtained on these films. Section III gives a brief review of the percolation model for the dc resistance and SAW attenuation. We compare the predictions of the percolation model to the experimental data in Sec. IV and discuss the details of the new calculations for the dc resistance. Finally, we summarize our results in Sec. V.

II. EXPERIMENTAL DATA

The data that were obtained on Pb/PbO_x and In/InO_x films are shown in Figs. 1 through 4. The data shown in Fig. 1 were obtained on a 500-Å-thick granular Pb/PbO_x film which had a normal-state resistance of 1000 Ω/□ (sample A). This film was produced by rf diode sputter deposition in an argon-oxygen atmosphere. The details of the deposition process, as well as the techniques used for measuring the dc resistance and SAW attenuation, have been reported in an earlier work.[4] After making the attenuation and resistance measurements, this film was oxidized in air to a normal-state sheet resistance of 1960 Ω/□ at which point the resistance and attenuation measurements were repeated. The data for the oxidized Pb/PbO_x film are shown in Fig. 2.

Figures 3 and 4 show the normalized SAW attenuation and the normalized dc resistance for two 100-Å-thick In/InO_x films. The normal-state sheet resistance for the film corresponding to the data shown in Fig. 3 (sample B) is 690 Ω/□ and the normal-state sheet resistance of the film corresponding to the data shown in Fig. 4 (sample C) is 3247 Ω/□. The In/InO_x films were produced by reactive ion-beam sputter deposition in an argon-oxygen at-

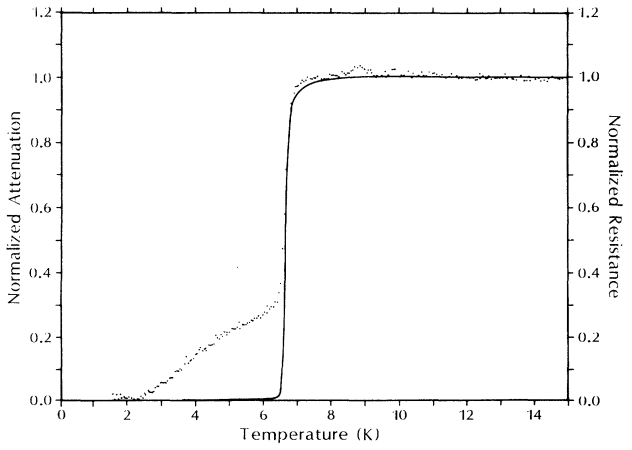

FIG. 1. Normalized resistance and normalized attenuation as a function of temperature for sample A.

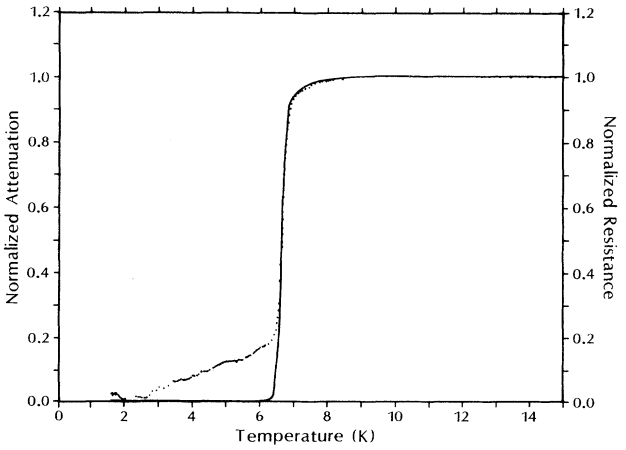

FIG. 2. Normalized attenuation and normalized resistance as a function of temperature for the oxidized granular Pb film.

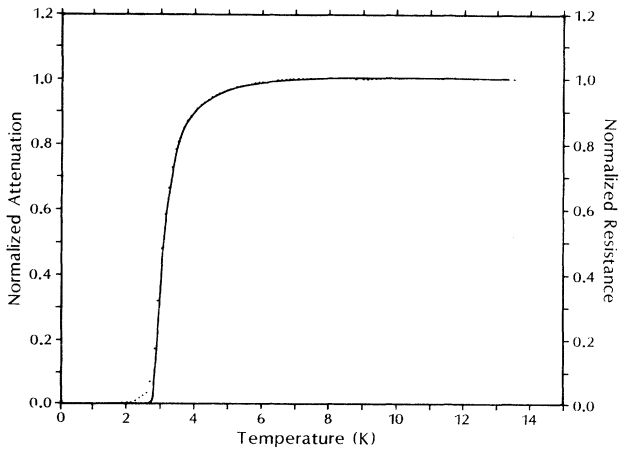

FIG. 4. Normalized attenuation and normalized resistance plotted as a function of temperature for sample C.

mosphere. The details of the deposition process for the In/InO_x films have also been reported in a previous work.[5] The structure of both the Pb/PbO_x and In/InO_x films were found to consist of pure metal grains embedded in an insulating matrix. The diameters of the metal grains are on the order of the film thickness, and electrical transport occurs by means of electron tunneling through the insulating barrier between neighboring grains.

The data shown in Figs. 1 through 4 show the same general features. As the film enters the superconducting state, we see that the SAW attenuation decreases to a minimum more slowly than the dc resistance. In addition, we see that, with the exception of the data shown in Fig. 4, there is a small "tail" in the resistive transition. Both of these features can be accounted for by the percolation model.

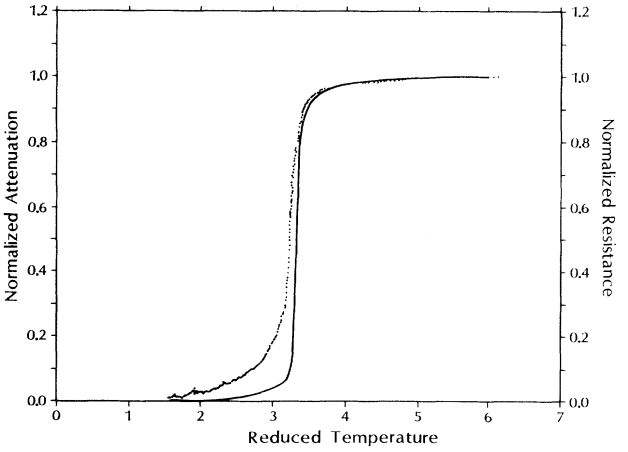

FIG. 3. Normalized attenuation and normalized resistance plotted as a function of temperature for sample B.

III. PERCOLATION DESCRIPTION OF GRANULAR SUPERCONDUCTING FILMS

In what follows, we present the major features of the percolation model. The details of the model can be found in Ref. 1. The basic assumption of the percolation model is that the long-range superconducting order is established in a granular film by means of classical percolation in a network of Josephson junctions. Under this assumption, the granular film can be represented as a random resistor network. The resistors of the network represent the Josephson junctions in the film and the nodes of the network represent the metallic grains. For simplicity, it is assumed that the nodes of the random resistor network form a square lattice. At temperatures below the superconducting transition temperature of the grains T_g, a fraction of the junction resistors in the network will have zero resistance due to tunneling of electron pairs across the insulating barrier between neighboring grains. As the temperature is lowered further, the fraction of zero-resistance junctions increases. When the fraction of zero-resistance junctions becomes equal to the critical percolation fraction (which occurs at a temperature $T_c < T_g$), a superconducting path is formed which traverses the film. At this point, the dc resistance of the film vanishes.

In the normal state, the junction resistances are assumed to have values which are distributed according to the function

$$W_n(r)=\frac{1}{r\ln(r_2/r_1)}\ , \tag{1}$$

where r_2 and r_1 are, respectively, the maximum and minimum values that the junction resistances can assume. However, for temperature below T_g, it was assumed (for simplicity) that the junction resistances were distributed according to the function

$$W_s(r)=p(T)\delta(r)+[1-p(T)\delta(r-R_n)]\ . \tag{2}$$

In (2), $p(T)$ is the (temperature-dependent) fraction of zero-resistance junctions and R_n is the normal-state sheet resistivity of the film. The temperature dependence of the resistance for temperatures less than T_g as predicted by the percolation model is found by using (2) in the effective-medium approximation.[6] The result of this substitution yields the following expression for the normalized resistance:

$$\frac{R(T)}{R_n}=\frac{1}{\ln(R_n/r_1)}\left[\ln\left[\frac{R_n}{r_J(T)}\right]\right] . \tag{3}$$

In (3), $r_J(T)$ is the critical value at which the junction resistance becomes equal to zero at the temperature T. That is, those junctions whose normal-state resistance is less than $r_J(T)$ will have zero resistance at the temperature T. The quantity $r_J(T)$ can be expressed in terms of experimentally measurable quantities as follows:

$$r_J(T)=\frac{\pi h\Delta(T)}{4e^2\gamma k_B T}\tanh\left[\frac{\Delta(T)}{2k_B T}\right] . \tag{4}$$

In (4) $\Delta(T)$ is the superconducting energy-gap function for the bulk material and γ is a constant on the order of unity. In addition, $r_J(T)$ can be related to $p(T)$ according to the following expression:

$$p(T)=\frac{\ln[r_J(T)/r_1]}{\ln(r_2/r_1)} . \tag{5}$$

Now consider the SAW attenuation in granular films. The attenuation that is being produced in these films is being produced by the acoustoelectric effect.[7] For a *homogeneous* film, the acoustoelectrically produced attenuation is given by[8,9]

$$\alpha_{ae}=\frac{\omega\kappa^2}{2}(\epsilon_s+\epsilon_0)R_\square , \tag{6}$$

where κ^2 is the electromechanical coupling constant of the substrate, ω is the angular frequency of the SAW, ϵ_s (ϵ_0) is the dielectric constant of the substrate (vacuum), and $R_\square$ is the sheet resistance of the film ($=\rho/d$, where ρ is the resistivity of the film and d is the film thickness). Equation (6) tells us that for homogeneous films, the SAW attenuation is proportional to the sheet resistivity of the film. However, for granular films this simple proportionality does not hold. This can be seen in two aspects of the data. First, as mentioned previously, the SAW attenuation decreases to a minimum more slowly than the resistance as the film becomes superconducting. Second, if one computes the SAW attenuation in the normal state using (6), it is found that the measured attenuation is always larger than that predicted by (6) (see Table I).

To account for the observed attenuation data, a reinterpretation of the results of Refs. 7 and 8 was proposed. This reinterpretation can be summarized as follows. When the fraction of zero-resistance junctions becomes equal to the critical percolation fraction, the dc resistance will vanish. The SAW attenuation, on the other hand, will remain nonzero because the SAW is not confined to follow the path of least resistance. The SAW will pass through those regions of the film that are still in the normal state and these normal regions will produce attenuation. Moreover, the magnitude of the attenuation will be proportional to the average sheet resistance of small sections of the film whose dimensions are on the order of the SAW wavelength. To see this, consider the following simple picture. The dc resistance measurement determines the response of the entire film to a dc potential, i.e., an ac potential of infinite wavelength. On the other hand, the alternating currents produced by the SAW as it propagates can be regarded as an ensemble of direct currents which sample the resistance of small sections of the film whose dimensions are on the order of the SAW wavelength. Since the granular films are inhomogeneous, the sheet resistance of these small sections of the film $R(L)$ of length L will vary from location to location. Hence, the SAW attenuation should be proportional to the average sheet resistance of these small sections $\overline{R(L)}$ and not the dc resistance. In the normal state the average resistance of these small sections is larger than the dc resistance and, thus, the observed attenuation should be larger than that predicted by (6).

Below T_g, the normalized SAW attenuation that is predicted by the percolation model is given by

$$\frac{\alpha(T)}{\alpha_n}\simeq\frac{\sigma}{\sqrt{2\pi}p}\exp\left[-\frac{(p-\tilde{p}_c)^2}{2\sigma^2}\right]-\left[\frac{(p-\tilde{p}_c)}{2p}\right]\times\left[1-\mathrm{erf}\left[\frac{(p-\tilde{p}_c)}{2\sigma}\right]\right] \tag{7}$$

for $p\equiv p(T)\simeq 1$, and

TABLE I. Various quantities defined in the text associated with three measured samples.

Sample	A	A(oxidized)	B	C
Normal-state sheet resistivity ($\Omega/\square$)	1000	1950	690	3247
Normal-state attenuation (dB/cm)	4.4	11.82	1.64	11.13
α_{ae} dB/cm	2.3	5.03	1.3	7.76
$r_1(\Omega)$	0.5	0.5	2.20	8.75
$r_2(\Omega)$	2.00×10^6	8.82×10^6	5.45×10^6	1.11×10^6
σ	3.3	3.3	12	0.05

$$\frac{\alpha(T)}{\alpha_n} \simeq 1 - \frac{p}{\tilde{p}_c} \tag{8}$$

for $p \simeq 0$. In Eqs. (6) and (7), σ and $\tilde{p}_0$ are given by

$$\sigma = \frac{1}{\ln(r_2/r_1)} \left[2 \ln \left[\frac{\alpha(\text{obs})}{\alpha_{ae}} \right] \right]^{1/2}, \tag{9}$$

$$\tilde{p}_c = p_c + \sigma^2 \ln(r_2/r_1), \tag{10}$$

where $p_c \equiv p(T_c)$ ($=0.5$ for a square lattice), $\alpha(\text{obs})$ is the observed normal-state attenuation, and α_{ae} is the normal-state attenuation predicted by Eq. (6).

IV. COMPARISON OF THE DATA TO THE PERCOLATION MODEL

In Figs. 5–8 we show the normalized SAW attenuation data and the normalized SAW attenuation as predicted by the percolation model for $T < T_g$ plotted as a function of reduced temperature (T/T_c). As can be seen, the agreement between the SAW attenuation data and the SAW attenuation predicted by the percolation model is quite good. In order to apply the percolation model to these films, the values of r_1, r_2, and σ must be determined. The value of r_1 was estimated to be equal to the resistance of a cube of pure metal (either Pb or In) whose dimensions were equal to the thickness of the film. The value of σ was determined from the temperature at which the dc resistance became equal to zero. According to (3), the dc resistance will vanish when $r_f(T_c) = R_n$. Using this condition in (4) allows us to solve for σ. The value of r_2 is determined by the condition[1]

$$r_2 = \frac{R_n^2}{r_1}. \tag{11}$$

The values of r_1, r_2, and σ for each of the samples are given in Table I, which also contains the experimental value for the normal-state attenuation, and the theoretical value obtained for this from the Adler model α_{ae}.

Figures 9–12 show the normalized resistance data

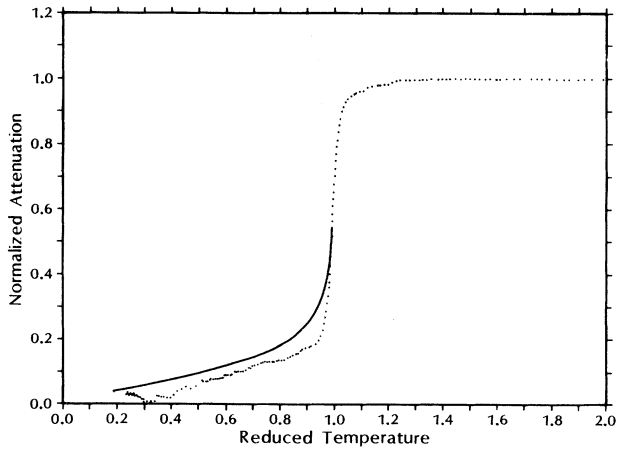

FIG. 6. Normalized attenuation data and the normalized attenuation as predicted by the percolation model as a function of reduced temperature for the oxidized granular Pb film.

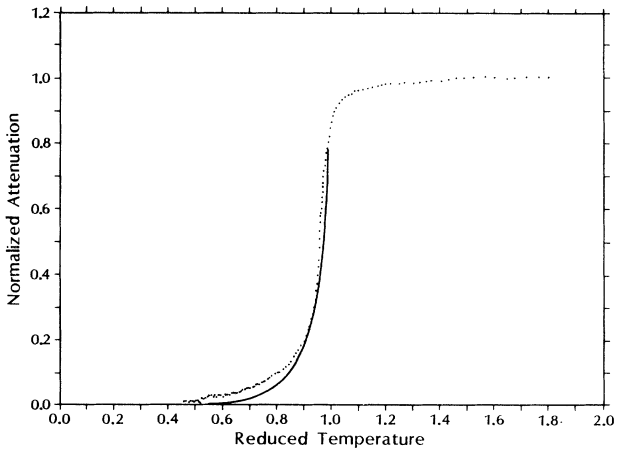

FIG. 7. Normalized attenuation data for sample B and the normalized attenuation as predicted by the percolation model.

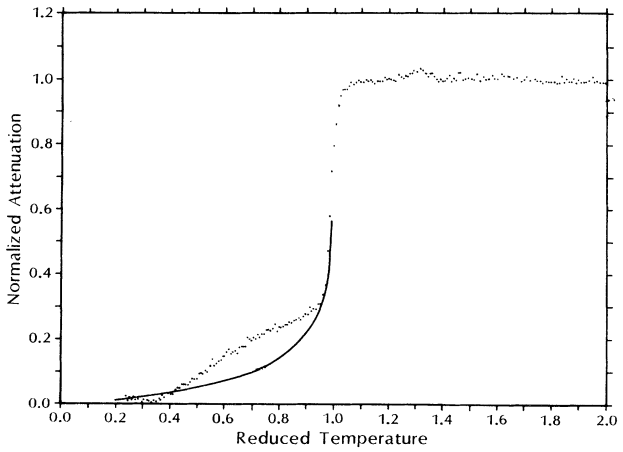

FIG. 5. Normalized attenuation data and the normalized attenuation predicted by the percolation model for sample A.

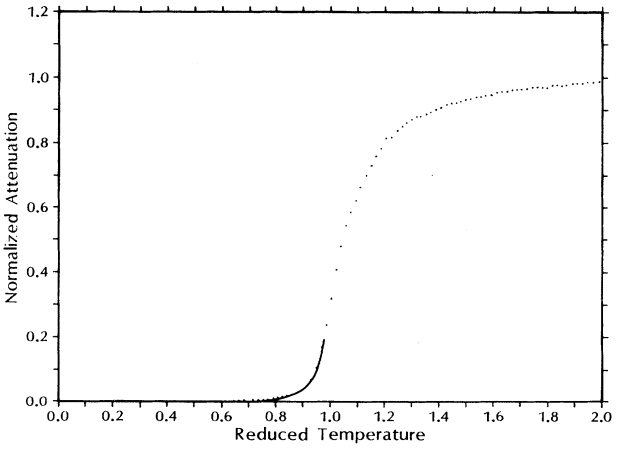

FIG. 8. Normalized attenuation data for sample C and the normalized attenuation predicted by the percolation model.

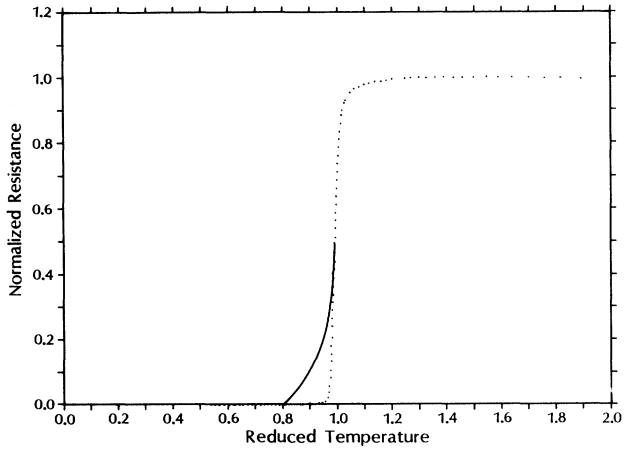

FIG. 9. Normalized resistance data (points) and the normalized resistance as predicted by the percolation model (solid curve) for sample A.

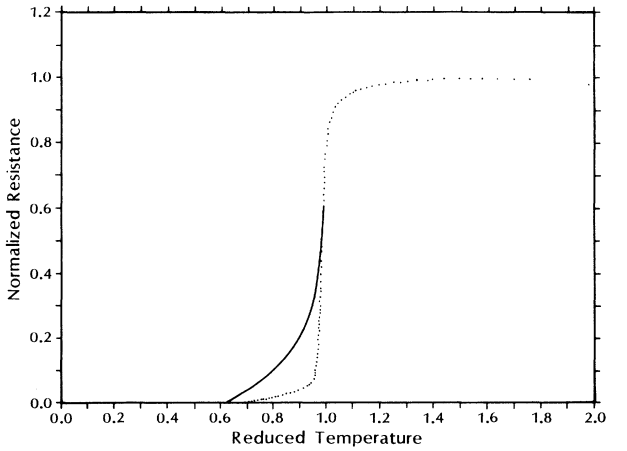

FIG. 11. Normalized resistance data (points) and the normalized resistance as predicted by the percolation model (solid curve) for sample B.

plotted as a function of reduced temperature and the normalized resistance as predicted by the percolation model. We see that, with the exception of sample C, the percolation model predicts a more gradual decrease in resistance than is seen experimentally. A possible explanation for the discrepancy between the data and the percolation model may lie in the assumptions that have been made. Recall that below T_g, the junction resistances were assumed to be distributed according to a binary distribution. Clearly, such a distribution is not realistic. A more realistic distribution function would be

$$\omega_s(r)=(1-p)W_n(r)+p\delta(r) , \tag{12}$$

where $W_n(r)$ is given by (1). Using (12) in the effective-medium approximation (see the Appendix), we see that the normalized resistance is now given by

$$\frac{R(T)}{R_n}=\left[\frac{r_2}{r_1}\right]^{p_2}\left[\frac{(r_2/r_1)^{1-p_1}-1}{(r_2/r_1)^{p_1}-1}\right] , \tag{13}$$

where $p_2=p/(2-2p)$ and $p_1=1/(2-2p)$. The solid curves in Figs. 13–16 indicate the normalized resistance as predicted by (13). As can be seen, this new calculation for the resistance appears to provide better agreement with the experimental data.

Two issues need to be addressed here. First, one might ask how does the distribution function (12) affect the predicted SAW attenuation? If (12) is used to compute the normalized SAW attenuation, the result is (see the Appendix)

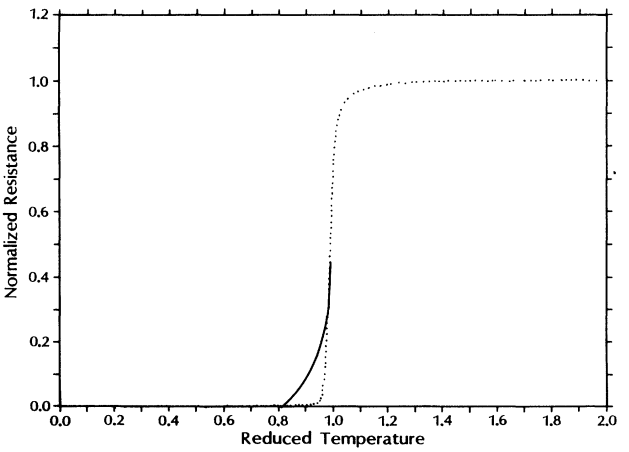

FIG. 10. Normalized resistance data (points) and the normalized resistance as predicted by the percolation model (solid curve) for the oxidized Pb/PbO_x film.

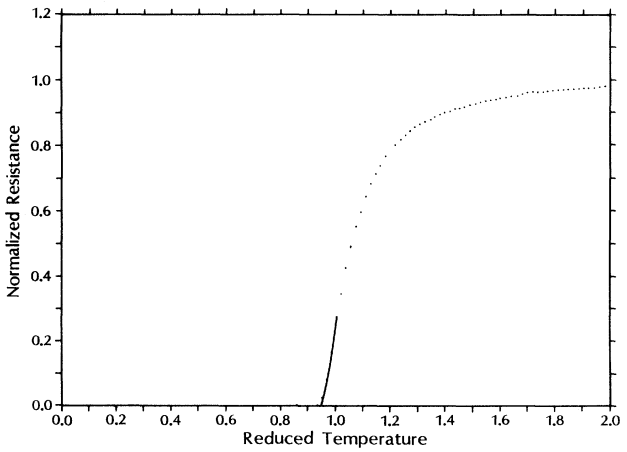

FIG. 12. Normalized resistance data (points) and the normalized resistance as predicted by the percolation model (solid curve) for sample C.

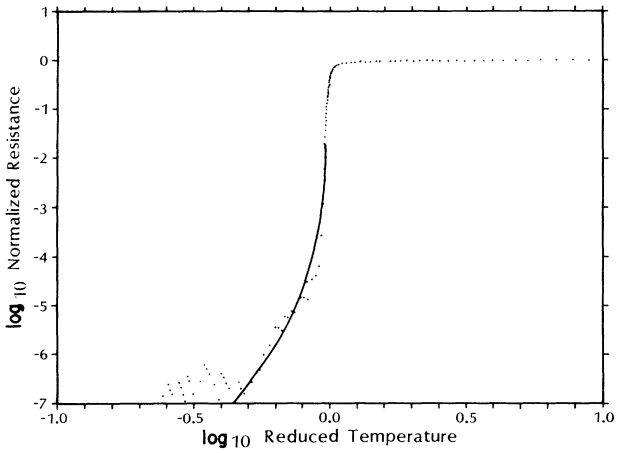

FIG. 13. Log-log plot of the normalized resistance data and the normalized resistance as predicted by Eq. (13) for the unoxidized granular Pb film.

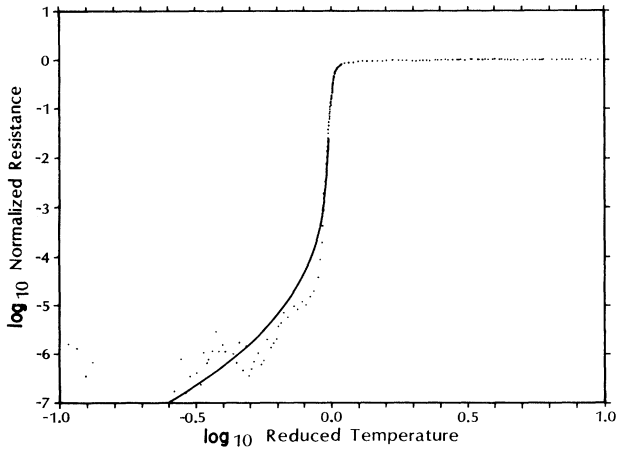

FIG. 14. Log-log plot of the normalized resistance data and the normalized resistance as predicted by Eq. (13) for the oxidized granular Pb film.

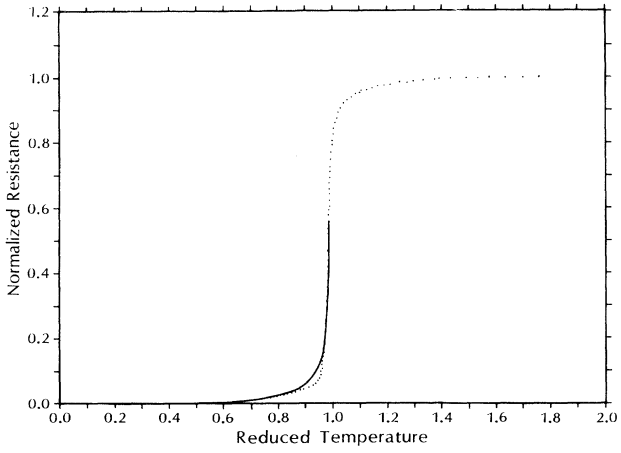

FIG. 15. Normalized resistance data for sample B (points) and the normalized resistance as predicted by the percolation model using the full distribution for the junction resistances (solid curve).

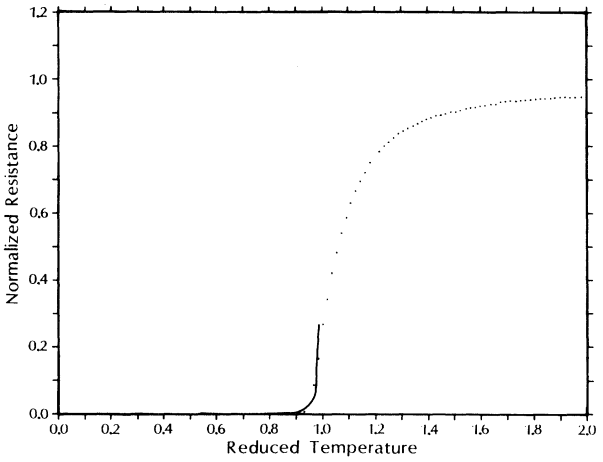

FIG. 16. Normalized resistance data for sample C (points) and the normalized resistance as predicted by the percolation model using the full distribution for the junction resistances (solid curve).

$$\frac{\alpha(T)}{\alpha_n}=\frac{r_1}{2\overline{R_n(L)}}\left[\left[\frac{r_2}{r_1}\right]^{p_3}\left[\frac{\overline{R_n(L)}}{R_n}\right]^{p_4}\operatorname{erfc}(z_1)-\operatorname{erfc}(x_1)\right]. \tag{14}$$

The quantities p_3, p_4, z, and x_1 are defined in the Appendix and $\overline{R_n(L)}$ is given by

$$\overline{R_n(L)}=R_n\exp\{\tfrac{1}{2}[\sigma\ln(r_2/r_1)]^2\}\ . \tag{15}$$

The normalized attenuation as predicted by (14) for sample A is indicated in Fig. 17 by the solid curve. As can be seen, the agreement between the attenuation data and the attenuation predicted by the percolation model when (12)

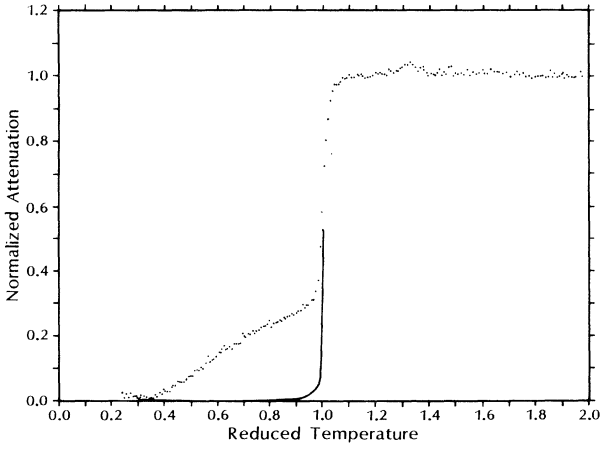

FIG. 17. Normalized attenuation data for sample A and the normalized attenuation as predicted by Eq. (14) (solid line).

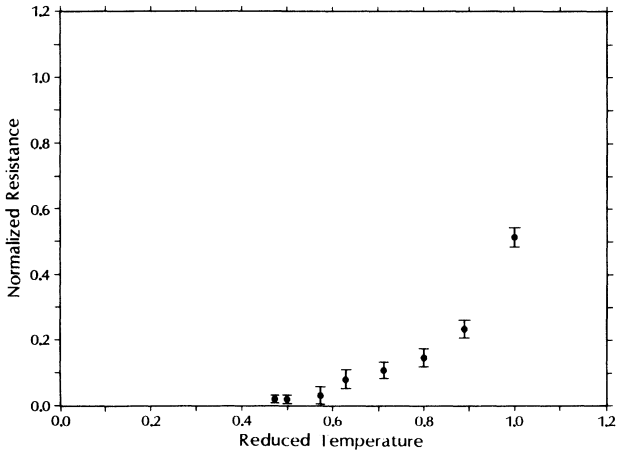

FIG. 18. Normalized resistance of a 16×16 resistor network as determined by computer simulations.

is used is not as good as the agreement between the attenuation data and the attenuation predicted by the percolation model when (2) is used. Similar behavior is seen for the other samples. This behavior should not be surprising since the distribution function for the junction resistances in a finite network is probably discontinuous. This would explain the fact that the agreement between the attenuation data and the percolation model is better when (2) is used. Some simple computer simulations[9] have shown that the binary distribution is not unreasonable for finite networks. In Fig. 18 we show the computer simulation for the average normalized resistance as a function of reduced temperature for a 16×16 node square lattice using (2). This lattice size corresponds to the size of the finite network for the granular Pb/PbO_x film. The data points represent the mean of 50 simulations and the error bars indicate a standard deviation about the mean. As can be seen, the computer simulations show a substantial tail in the resistive transition of the finite networks. Since the normalized SAW attenuation is proportional to the average resistance of the finite networks, the computer simulations seem to indicate that the binary distribution is not too unreasonable for the finite networks.

V. SUMMARY

In this paper we have reported on the measurements of the SAW attenuation and dc resistance made on granular Pb/PbO_x and granular In/InO_x films. The data obtained on these films displayed the same tendency—the SAW attenuation decreased to zero more slowly than the dc resistance as the films entered the superconducting state. We have found that the behavior described above can be explained in terms of a model which is based on a percolation theory of granular superconductors. Within the scope of this model, the fact that the resistance decreases to zero more slowly than the dc resistance is due to the fact that the SAW is sensitive to the resistance of small sections of the film which can have local average resistances that are larger than the measured dc resistance. We also find that in addition to explaining the above effect, the percolation model can qualitatively account for the shapes of the attenuation and resistance curves.

ACKNOWLEDGMENTS

The work at the University of Wisconsin–Milwaukee was supported by the U.S. Office of Naval Research.

APPENDIX

Here we consider the effects of using the effective-medium approximation for $T > T_g$ and $T < T_g$. The approach that is used is to replace the Ambegaokar, Halperin, and Langer (AHL) model[10] used in Ref. 1 by the effective-medium approximation[6] (EMA) when the sample enters the superconducting state. In the context of the present problem, the EMA states that the effect of shorting out some of the resistors of the network is equivalent to giving *all* of the resistors of the network a single value R_{eff} which is equal to the effective sheet resistance of the network. R_{eff} is chosen so that the effects of changing a given resistor back to its original value will, on the average, cancel out. Specifically, R_{eff} is given by solving the following integral equation:

$$0=\int W(r)\left[\frac{R_{\text{eff}}-r}{R_{\text{eff}}+\phi r}\right]dr \ . \tag{A1}$$

In (A1) $W(r)$ is the actual resistance distribution and $\phi=z/2-1$ where z is the coordination number. The coordination number is the number of nearest neighbors associated with a given node in the resistor network (for a square lattice $z=4$). The coordination number is related to the critical percolation fraction according to $P_c=2/z$.

Consider the normal state first. Substituting the distribution for the junction resistances in the normal state Eq. (1) into (A1), we obtain

$$0=\int_{r_1}^{r_2}\frac{1}{r}\left[\frac{r-R_n}{R_n+\phi r}\right]dr \ , \tag{A2}$$

$$0=\int_{r_1}^{r_2}\frac{dr}{R_n+\phi r}-R_n\int_{r_1}^{r_2}\frac{dr}{r(R_n+\phi r)} \ , \tag{A3}$$

$$0=\frac{1}{\phi}\ln\left[\frac{R_n+\phi r_2}{R_n+\phi r_1}\right]+\ln\left[\frac{R_n+\phi r_1}{r_2}\right] -\ln\left[\frac{R_n+\phi r_1}{r_1}\right] , \tag{A4}$$

$$\frac{\phi}{\phi+1}\ln(r_2/r_1)=\ln\left[\frac{R_n+\phi r_2}{R_n+\phi r_1}\right] . \tag{A5}$$

Since $\phi=z/2-1$, we have $\phi/(\phi+1)=1-z/2$. Moreover, since $p_c=2/z$, we have $\phi/(\phi+1)=1-p_c$. Exponentiating both sides of (A5), we obtain

$$(r_2/r_1)^{1-p_c}=\frac{R_n+\phi r_2}{R_n+\phi r_1} \ . \tag{A6}$$

Solving (A6) for R_n, we obtain

$$R_n=\phi r_1(r_2/r_1)^{1-p_c}\left[\frac{(r_2/r_1)^{p_c}-1}{(r_2/r_1)^{1-p_c}-1}\right] . \quad \text{(A7)}$$

For a square lattice, $\phi=1$ and $p_c=\frac{1}{2}$. In this case, (A7) reduces to

$$R_n=(r_1r_2)^{1/2} \quad \text{(A8)}$$

which is the same result as Eq. (11) which was derived from the AHL model. Thus, we see that, at least for a square lattice, the AHL model can be replaced by the effective-medium approximation.

Let us now consider what happens when $T<T_g$. In particular, we will consider the case when the binary distribution for the junction resistances Eq. (2) is replaced by a more "realistic" distribution function. The distribution that we shall use is

$$w_s(r)=(1-p)W_n(r)+p\delta(r-0) , \quad \text{(A9)}$$

where p is the fraction of superconducting junctions given by Eq. (5) and $W_n(r)$ is given by Eq. (1). Substitution of (A9) into (A1) yields

$$0=A(1-p)\int_{r_1}^{r_2}\frac{1}{r}\left[\frac{r-R(T)}{R(T)-\phi r}\right]dr-p , \quad \text{(A10)}$$

where $A=[\ln(r_2/r_1)]^{-1}$. Performing the integration, we obtain

$$\frac{1}{1-p}\ln(r_2/r_1)=\frac{1}{1-p_c}\ln\left[\frac{R(T)+\phi r_2}{R(T)+\phi r_1}\right] . \quad \text{(A11)}$$

Multiplying both sides of (A11) by $1-p_c$ and exponentiating, we obtain

$$(r_2/r_1)^{p_1}=\frac{R(T)+\phi r_2}{R(T)+\phi r_1} , \quad \text{(A12)}$$

where $p_1=(1-p_c)/(1-p)$. Solving (A12) for $R(T)$ yields

$$R(T)=\phi r_1(r_2/r_1)^{p_1}\left[\frac{(r_2/r_1)^{1-p_1}-1}{(r_2/r_1)^{p_1}-1}\right] . \quad \text{(A13)}$$

Equation (A13) is the most general expression for the resistance in the region $T<T_g$. We see that when $p=0$, $p_1=1-p_c$, and (A13) reduces to (A7), that is, $R(T)=R_n$. When $p=p_c$, then $p_1=1$ and $R(T)=0$.

For simplicity, let us restrict the remainder of this discussion to the case of a square resistor network so that $p_1=1/(2-2p)$ and $R_n=r_1(r_2/r_1)^{1/2}$. Dividing both sides of (A13) by R_n, we obtain

$$\frac{R(T)}{R_n}=(r_2/r_1)^{p_2}\left[\frac{(r_2/r_1)^{1-p_1}-1}{(r_2/r_1)^{p_1}-1}\right] , \quad \text{(A14)}$$

where $p_2=p/(2-2p)$. In addition, if $r_2\gg r_1$, then the denominator is approximately equal to $(r_2/r_1)^{p_1}$ and (A14) reduces to

$$\frac{R(T)}{R_n}=(r_2/r_1)^{1/2}[(r_2/r_1)^{1-p_1}-1] . \quad \text{(A15)}$$

Next, let us consider what effect (A9) will have on the attenuation [or, more specifically, $R(L,T)$] in the region $T<T_g$. To compute $R(L,T)$, we first write r_2/r_1 in terms of R_n. Upon doing so, (A15) becomes

$$R(T)=r_1[(R_n/r_1)^{(1-p_1)/p_c}-1] . \quad \text{(A16)}$$

We then follow the procedure described in Ref. 1, Sec. III; we replace R_n by $R_n(L)$ and p_c by p_L. Under this substitution, (A16) becomes

$$R(L,T)=r_1\{[R_n(L)/r_1]^{(1-p_1)/p_L}-1\} . \quad \text{(A17)}$$

The average resistance of the finite networks is then

$$\overline{R(L,T)}=\int_{p(T)}^{1}R(L,T)\Phi_L(p_L)dp_L , \quad \text{(A18)}$$

where $\Phi_L(p_L)$ is given by Eq. (14), Ref. 1. Substituting the expression for $\Phi_L(p_L)$ and $R(L,T)$ into (A18), we obtain

$$\begin{aligned}\overline{R(L,T)}=&\frac{r_1}{\sqrt{2\pi}\sigma_L}\int_{p(T)}^{1}[R_n(L)/r_1]^{(1-p_1)/p_L}\\&\times\exp\left[-\frac{(p_L-p_c)^2}{2\sigma_L^2}\right]dp_L\\&+\frac{r_1}{\sqrt{2\pi}\sigma_L}\int_{p(T)}^{1}\exp\left[-\frac{(p_L-p_c)^2}{2\sigma_L^2}\right]dp_L\\=&I_1+I_2 . \quad \text{(A19)}\end{aligned}$$

Consider the second integral (I_2). Because of the nature of the integrand, we can extend the upper limit of integration to infinity. We then have

$$I_2=\frac{r_1}{\sqrt{2\pi}\sigma_L}\int_{p(T)}^{\infty}\exp\left[-\frac{(p_L-p_c)^2}{2\sigma_L^2}\right]dp_L . \quad \text{(A20)}$$

Making the change in variable $x=(p_L-p_c)/(\sqrt{2}\sigma_L)$, (A20) becomes

$$I_2=\frac{r_1}{\sqrt{\pi}}\int_{x_1}^{\infty}e^{-x^2}dx , \quad \text{(A21)}$$

where $x_1=[p(T)-p_c]/(\sqrt{2}\sigma_L)$. The integrand in (A21) is related to the error function. Thus

$$I_2=\frac{r_1}{2}[1-\mathrm{erf}(x_1)] . \quad \text{(A22)}$$

Now consider the first integral (I_1). Since the argument of the integral contains a decreasing exponential, we can extend the upper limit of integration to infinity without any complications. Hence

$$\begin{aligned}I_1=&\frac{r_1}{\sqrt{2\pi}\sigma_L}\int_{p(T)}^{\infty}[R_n(L)/r_1]^{(1-p_1)/p_L}\\&\times\exp\left[-\frac{(p_L-p_c)^2}{2\sigma_L^2}\right]dp_L . \quad \text{(A23)}\end{aligned}$$

Using Eq. (18) in Ref. 1, we can rewrite (A23) as

$$I_1=\frac{r_1}{\sqrt{2\pi}\sigma_L}\int_{p(T)}^{\infty}\exp\left[\left[\frac{p_L-p}{1-p}\right]\ln(r_2/r_1)-\frac{1}{2\sigma_L^2}(p_L^2-2p_cp_L+p_c^2)\right]dp_L\ . \tag{A24}$$

Completing the square in the argument of the exponential and using Eq. (20), Ref. 1, we obtain

$$I_1=\frac{r_1}{\sqrt{2\pi}\sigma_L}\int_{p(T)}^{\infty}\left[\frac{r_2}{r_1}\right]^{p_3}\left[\frac{\overline{R_n(L)}}{R_n}\right]^{p_4}\times\exp\left[-\frac{(p_L-\tilde{p}_c)^2}{2\sigma_L^2}\right]dp_L\ , \tag{A25}$$

where

$$\tilde{p}_c=p_c-\frac{\sigma_L^2}{1-p}\ln(r_2/r_1)\ ,$$

$p_3=(p_c-p)/(1-p)$, and $p_4=(1-p)^{-2}$. The first two factors of the integrand do not depend upon p_L and can be taken outside of the integral. Making the change in variable $Z=(p_L-\tilde{p}_c)/(\sqrt{2}\sigma_L)$, (A25) becomes

$$I_1=\frac{r_1}{\sqrt{\pi}}\left[\frac{r_2}{r_1}\right]^{p_3}\left[\frac{\overline{R_n(L)}}{R_n}\right]^{p_4}\int_{z_1}^{\infty}e^{-z^2}dz \tag{A26}$$

$$=\frac{r_1}{2}\left[\frac{r_2}{r_1}\right]^{p_3}\left[\frac{\overline{R_n(L)}}{R_n}\right]^{p_4}[1-\mathrm{erf}(z_1)]\ , \tag{A27}$$

where $z_1=[p(T)-\tilde{p}_c]/(\sqrt{2}\sigma_L)$. Thus, (A19) becomes

$$R(L,T)=\frac{r_1}{2}\left[\left[\frac{r_2}{r_1}\right]^{p_3}\left[\frac{\overline{R_n(L)}}{R_n}\right]^{p_4}[1-\mathrm{erf}(z_1)]-[1-\mathrm{erf}(x_1)]\right]\ . \tag{A28}$$

The normalized attenuation for $T<T_g$ is then

$$\frac{\alpha(T)}{\alpha_n}=\frac{r_1}{2\overline{R_n(L)}}\left[\left[\frac{r_2}{r_1}\right]^{p_3}\left[\frac{\overline{R_n(L)}}{R_n}\right]^{p_4}\mathrm{erfc}(z_1)-\mathrm{erfc}(x_1)\right]\ , \tag{A29}$$

where $\mathrm{erfc}(x)=1-\mathrm{erf}(x)$ is the complementary error function.

---

*Present address: AT&T Bell Laboratories, Naperville, Illinois 60506.

[1]M. Levy, J. Schmidt, A. Schenstrom, M. Revzen, A. Ron, B. Shapiro, and C. G. Kuper, Phys. Rev. B **34**, 1508 (1986).

[2]G. Deutscher, O. Entin-Wohlman, S. Fishman, and Y. Shapira, Phys. Rev. B **21**, 5041 (1980).

[3]O. Entin-Wohlman, A. Kapitulnik, and Y. Shapira, Phys. Rev. B **24**, 6464 (1981).

[4]H. Tejima, J. Schmidt, C. Figura, and M. Levy, *1983 IEEE Ultrasonics Symposium Proceedings,* edited by B. R. McAvoy (IEEE, New York, 1983), p. 1100.

[5]A. F. Hebard and A. T. Fiory, Phys. Rev. Lett. **58**, 1131 (1978).

[6]For a general discussion of the effective-medium approximation, see S. Kirkpatrick, Phys. Rev. Lett. **27**, 1722 (1971).

[7]K. A. Ingebrigtsen, J. Appl. Phys. **40**, 2681 (1969).

[8]K. A. Ingebrigtsen, J. Appl. Phys. **41**, 454 (1970).

[9]J. Schmidt, Ph.D. thesis, University of Wisconsin-Milwaukee, 1987.

[10]V. Ambegaokar, B. I. Halperin, and J. S. Langer, Phys. Rev. B **24**, 2612 (1971).